

Efficient ion acceleration driven by a Laguerre-Gaussian laser in near-critical-density plasma

Jia-Xiang Gao(高嘉祥) Meng Liu(刘梦), and Wei-Min Wang(王伟民)
Citation: Chin. Phys. B, 2023, 32 (**10**): 105202. DOI: 10.1088/1674-1056/ace428
Journal homepage: http://cpb.iphy.ac.cn; http://iopscience.iop.org/cpb

What follows is a list of articles you may be interested in

Effect of sharp vacuum-plasma boundary on the electron injection and acceleration in a few-cycle laser driven wakefield

Guo-Bo Zhang(张国博), Song Liu(刘松), De-Bin Zou(邹德滨), Ye Cui(崔野), Jian-Peng Liu(刘建鹏), Xiao-Hu Yang(杨晓虎), Yan-Yun Ma(马燕云), and Fu-Qiu Shao(邵福球)
Chin. Phys. B, 2023, 32 (**9**): 095202. DOI: 10.1088/1674-1056/acdc0c

Electron acceleration during magnetic islands coalescence and division process in a guide field reconnection

Shengxing Han(韩圣星), Huanyu Wang(王焕宇), and Xinliang Gao(高新亮)
Chin. Phys. B, 2022, 31 (**2**): 025202. DOI: 10.1088/1674-1056/ac21c0

Optimization of the beam quality in ionization injection by a tailoring gas profile

Ye Cui(崔野), Guo-Bo Zhang(张国博), Yan-Yun Ma(马燕云), Xiao-Hu Yang(杨晓虎), Jia-Yin Mu(牟佳胤), Hai-Bo Yao(姚海波), Ming Zi(资明), Jie Zhou(周洁), Jing-Qi Yang(杨静琦), Li-Xiang Hu(胡理想), and Li-Chao Tian(田立朝)
Chin. Phys. B, 2021, 30 (**10**): 105201. DOI: 10.1088/1674-1056/ac1b89

Nonlinear propagation of an intense Laguerre-Gaussian laser pulse in a plasma channel

Mingping Liu(刘明萍), Zhen Zhang(张震), and Suhui Deng(邓素辉)
Chin. Phys. B, 2021, 30 (**5**): 055204. DOI: 10.1088/1674-1056/abd68c

Spontaneous growth of the reconnection electric field during magnetic reconnection with a guide field: A theoretical model and particle-in-cell simulations

Kai Huang(黄楷), Quan-Ming Lu(陆全明), Rong-Sheng Wang(王荣生), Shui Wang(王水)
Chin. Phys. B, 2020, 29 (**7**): 075202. DOI: 10.1088/1674-1056/ab8da0

Efficient ion acceleration driven by a Laguerre–Gaussian laser in near-critical-density plasma

Jia-Xiang Gao(高嘉祥)[1] Meng Liu(刘梦)[2,†], and Wei-Min Wang(王伟民)[1,3,4,‡]

[1] *Department of Physics and Beijing Key Laboratory of Optoelectronic Functional Materials and Micronano Devices, Renmin University of China, Beijing* 100872, *China*

[2] *Department of Mathematics and Physics, North China Electric Power University, Baoding* 071003, *China*

[3] *Key Laboratory of Quantum State Construction and Manipulation (Ministry of Education), Renmin University of China, Beijing* 100872, *China*

[4] *IFSA Collaborative Innovation Center, Shanghai Jiao Tong University, Shanghai* 200240, *China*

(Received 13 May 2023; revised manuscript received 22 June 2023; accepted manuscript online 5 July 2023)

Laser-driven ion accelerators have the advantages of compact size, high density, and short bunch duration over conventional accelerators. Nevertheless, it is still challenging to generate ion beams with quasi-monoenergetic peak and low divergence in experiments with the current ultrahigh intensity laser and thin target technologies. Here we propose a scheme that a Laguerre–Gaussian laser irradiates a near-critical-density (NCD) plasma to generate a quasi-monoenergetic and low-divergence proton beam. The Laguerre–Gaussian laser pulse in an NCD plasma excites a moving longitudinal electrostatic field with a large amplitude, and it maintains the inward bowl-shape for dozens of laser durations. This special distribution of the longitudinal electrostatic field can simultaneously accelerate and converge the protons. Our particle-in-cell (PIC) simulation shows that the efficient proton acceleration can be realized with the Laguerre–Gaussian laser intensity ranging from 3.9×10^{21} W·cm^{-2}–1.6×10^{22} W·cm^{-2} available in the near future, e.g., a quasi-monoenergetic proton beam with peak energy $\sim$ 115 MeV and divergence angles less than 5° can be generated by a 5.3×10^{21} W·cm^{-2} pulse. This work could provide a reference for the high-quality ion beam generation with PWclass laser systems available recently.

Keywords: Laguerre–Gaussian laser, laser-driven ion acceleration, particle-in-cell simulations, near-critical-density plasma

PACS: 52.38.Kd, 52.65.Rr, 41.75.Jv **DOI:** 10.1088/1674-1056/ace428

1. Introduction

With the recent rapid development of ultrashort ultraintense lasers, proton beams with cutoff energy of near 100 MeV can be generated from the interaction of intense lasers with solid foils.[1–4] A few features of the laserdriven ion accelerator, including higher ion density and shorter bunch or more compact size,[5,6] can be applied in various prospective areas, covering proton radiography for cancer treatment,[7] fast ignition of nuclear fusion,[8] and nuclear physics,[9,10] etc. However, a quasi-monoenergetic beam with low divergence,[11] is still a critical requirement for most of these attractive applications under the present laboratory conditions. Usually, the proton beams have a divergence up to tens of degrees generated in experiments.[12–14]

To overcome this limitation, significant efforts have been devoted to concentrate the transversely distributed proton beam at the center. For instance, funnel-like target,[15] curved targets,[16] density-modulated targets embedded in a substrate thick enough,[17] and plane targets with rectangular and cylindrical geometries at the back,[18] have been widely used to control the ion trajectory near the laser propagation axis. Improving the beam focusing properties will enable the charge-separated fields on the surface of the structure targets to efficiently guide proton beams. In addition, a new type of movable electrostatic field with a helical wire excited by laser irradiating on a target can concentrate and accelerate the protons inside simultaneously.[19] However, the application of these laser-driven proton beams is restricted by the expense of the complex assembled target. It is highly desired to promote simple methods to generate a quasi-monoenergetic proton beam with low divergence for the coming petawatt (PW) laser systems. Recently, with the application of supersonic gas jet and nanosecond laser reshaping technology, the manufacture of a near-critical-density (NCD) plasma has made remarkable progress,[20–24] and there are some experimental results of laser-driven ion acceleration based on laser NCD plasmas interaction.[24,25]

In this paper, we propose to adopt a relativistic Laguerre–Gaussian (LG) laser pulse with an intrinsic hollow intensity distribution to accelerate and focus a proton beam in a near-critical-density (NCD) target. Such an LG laser pulse with an intensity above 10^{19} W·cm^{-2} has been available,[26] and even a higher intensity LG laser of 10^{22} W·cm^{-2} could be delivered from the SULF 10 PW and SEL 100-PW laser facilities in the coming few years.[27] With the intensity ranging from 10^{21} W·cm^{-2}–10^{22} W·cm^{-2}, simulation results show that the hollow structure of the LG laser can compress the plasma at

†Corresponding author. E-mail: liumeng@ncepu.edu.cn
‡Corresponding author. E-mail: weiminwang1@ruc.edu.cn

© 2023 Chinese Physical Society and IOP Publishing Ltd

the center.[28] In this paper, we find that quasi-monoenergetic proton beams can be efficiently generated when an LG laser pulse interacts with an NCD target. The relativistic laser pulse can excite a large-amplitude longitudinal electrostatic field to accelerate the protons forward. Meanwhile, the centripetal distribution of this longitudinal electrostatic field substantially converges the protons near the laser propagating axis. While a conventional Gaussian laser pulse with the same intensity irradiates on an NCD plasma, the generated proton beam is usually non-monoenergetic in our PIC simulations. Moreover, the peak energy and the corresponding proton yields using the LG laser are higher than the case with the Gaussian laser pulse.

2. Vacuum field structure of a helical laser pulse

To obtain ultra-relativistic intensity LG laser pulse, a spirally varying thickness for the spiral phase plate should be used.[26] By making a paraxial approximation to the wave equation of LG laser in cylindrical coordinates, one can obtain the eigen solution of Laguerre Gaussian beam wave equation as follows:[29]

$$\begin{aligned} &u(r,\varphi,x)\\ &= \frac{C_l^p}{w(x)}\left(\frac{\sqrt{2}r}{w(x)}\right)^{|l|}\exp\left(-\frac{r^2}{w^2(x)}\right)\\ &\times L_p^{|l|}(\zeta)\exp\left(-\mathrm{i}k\frac{r^2}{2R(x)}\right)\mathrm{e}^{(-\mathrm{i}l\varphi)}\,\mathrm{e}^{(-\mathrm{i}kx)}\,\mathrm{e}^{[\mathrm{i}\Psi(x)]}. \end{aligned} \tag{1}$$

The laser is incident at the position $x=0$ and propagates along the $+x$ direction. r is the distance from a spatial arbitrary point to the x axis. φ is the rotating angle around the x axis. l is the azimuthal quantum number, which can take any integer. p is the radial quantum number, which can take any integer greater than or equal to 0. And $p<|l|$ should be required. All l and p together constitute a set of orthogonal complete LG_{lp} basis vectors, which can represent any spatial mode. For example, the vortex laser with ultra-relativistic laser intensity in the experiment mentioned above is obtained by the superposition of several low-order LG lasers in the form of incoherent superposition.[30] The Laguerre polynomial $L_p^l(\zeta)$ is

$$\begin{aligned} &L_p^l(\zeta)=\sum_{k=0}^{p}\frac{(l+p)!(-)^k}{(l+k)!k!(p-k)!},\\ &\zeta=\frac{2r^2}{w_{l,p}(x)^2},\quad C_l^p=\sqrt{\frac{2p!}{\pi(p+|l|)!}}, \end{aligned} \tag{2}$$

where the C_l^p is the normalized constant, $w_{l,p}(x)=w_0\sqrt{1+(x/x_\mathrm{R})^2}$ is the beam waist at x position, w_0 is the beam waist on the focal plane ($x=0$), $x_\mathrm{R}=\pi w_0^2/\lambda$ is the Rayleigh range. The beam waist $w_{l,p}(x)$, the curvature radius $R(x)$, the Gouy phase $\Psi(x)_\mathrm{LG}$, and the far field divergence angle $\theta_{l,p}$ are expressed as follows:

$$\begin{aligned} &w_{l,p}(x)=\sqrt{|l|+2p+1}w_\mathrm{g}(x),\quad R(x)=x\left[1+\left(\frac{x_\mathrm{R}}{x}\right)^2\right],\\ &\Psi(x)_\mathrm{LG}=(|l|+2p+1)\arctan\left(\frac{x}{x_\mathrm{R}}\right),\\ &\theta_{l,p}=\sqrt{|l|+2p+1}\theta_\mathrm{g}, \end{aligned} \tag{3}$$

where the beam waist $w_\mathrm{g}(x)$ and far-field divergence angle θ_g are the TEM_{00} (transverse electromagnetic mode) of LG laser. According to Eq. (3), as the angular quantum number $|l|$ and radial quantum number p increase, the beams diverge faster and faster as the propagation distance increases. Thus, the pulse energy of the high-order LG laser losses faster than the low-order LG laser. And a high-order LG laser is also more difficult to produce. So in this paper, we adopted the TEM_{00} ($l=0$, $p=0$), i.e., Gaussian pulse, and the low-order TEM_{10} ($|l|=1$, $p=0$) LG pulse.

The amplitude profile of LG laser (a_LG) and Gaussian laser (a_G) is

$$\begin{aligned} a_\mathrm{LG}(t,r,x;l) &= a_0\cdot\exp\left(-\frac{t^2}{\tau^2}\right)\cdot\exp\left(-\frac{r^2}{w_\mathrm{R}^2}\right)\\ &\times\left(\frac{\sqrt{2}\cdot r}{w_\mathrm{R}}\right)^{|l|}\cdot L_p^l(\zeta),\\ a_\mathrm{G}(t,r) &= a_0\cdot\exp\left(-\frac{t^2}{\tau^2}\right)\cdot\exp\left(-\frac{r^2}{w_\mathrm{R}^2}\right), \end{aligned} \tag{4}$$

where a_0 is the normalized laser amplitude, $T=\lambda/c$ is the laser period, τ is the pulse duration, $r=\sqrt{z^2+y^2}$ is the distance from an arbitrary point in the space to the x axis, $w_\mathrm{R}=w_0\sqrt{1+\left(x_\mathrm{spot}/x_\mathrm{R}\right)^2}$ is the laser spot size at the $x=0$ interface of the simulation domain, w_0 is the laser focal spot radius, and x_spot is the position of laser focus on the x axis. When the energy, pulse duration, and focal spot of an LG laser pulse are the same as those of a Gaussian laser, the LG peak amplitude $a_0=a_0'\times(1-1/\mathrm{e})\approx 0.63a_0'$,[31] here a_0' is the input laser amplitude in our simulations. Therefore, in this paper, the LG laser and Gaussian laser used the same laser amplitude a_0. Besides, the phase of the LG laser and Gaussian laser is also different:

$$\begin{aligned} &\Phi_\mathrm{LG}=|l|\cdot\varphi+k_0\left(x_\mathrm{spot}+\frac{y^2}{2R_\mathrm{C}}\right)-\Psi(x)_\mathrm{LG},\\ &\Phi_\mathrm{G}=\frac{2\pi}{\lambda}\cdot\frac{y^2}{2R_\mathrm{C}}-\Psi(x)_\mathrm{G}. \end{aligned} \tag{5}$$

Equation (5) depicts that the LG laser has a helical phase varying with φ. $\Psi(x)_\mathrm{G}=\arctan(x/x_\mathrm{R})$ is the Gaussian laser Gouy phase.

The electric field of the LG laser in cylindrical coordinates is as follows:[32–34]

$$E_\mathrm{LG}(r,x;l)=E_0\cdot\exp\left(-\frac{r^2}{w_\mathrm{R}^2}\right)\cdot\left(\frac{\sqrt{2}\cdot r}{w_\mathrm{R}}\right)^{|l|}\cdot L_p^l(\zeta), \tag{6}$$

where $p=0$, $L_0^l(\zeta)=1$ is independent l. In this case, the transverse component perpendicular to the direction of propagation can be represented as

$$E_\perp(r,\varphi,x;l,\sigma)$$

$$= \frac{E_{\rm LG}(r,x;l)\left[\sin(\eta+l\varphi)\hat{y}-\sigma\cdot\cos(\eta+l\varphi)\hat{z}\right]}{\sqrt{2}}. \quad (7)$$

Here $\eta = kx+(kr^2/2R_{\rm C})-\Psi(x)$, and the longitudinal component parallel to the laser propagation direction is

$$E_{\parallel}(r,\varphi,x;l,\sigma) = E_{\rm LG}(r,x;l)\left[\frac{|l|-ls-2r^2/w(x)^2}{kr}\right] \times\cos[\eta+(l-\sigma)\varphi]\hat{x}. \quad (8)$$

A circularly polarized (CP) laser carries a spin angular momentum of $\sigma = 1$. Here $\sigma = 1$ and $\sigma = -1$ represent the left-handed CP laser and the right-handed CP laser, respectively.[35] Besides, each photon in the LG beam carries an orbital angular momentum (OAM) of $l\hbar$.[36] Thus, the total angular momentum of each photon is $\boldsymbol{J} = \boldsymbol{L}+\boldsymbol{S}$, that is, each photon carries a total angular momentum of $(l-\sigma)\hbar$. In order to guarantee the LG pulse has an inward ponderomotive force and does not transfer its angular momentum to the protons during the interaction between the laser and an NCD plasma, the angular momentum of photons should equal 0.[37]

With the parameters of $a_0 = 100$, $l = \pm 1$, $p = 0$, $\sigma = 1$, $w_0 = 7$ μm, we performed 2D PIC simulations for the LG laser interacting with an NCD plasma density of $n_{\rm e} = 10n_{\rm c}$. The result indicates that the LG laser of $l = \sigma = 1$ can gain better acceleration when the laser only has focusing pondermotive force and will not transfer angular momentum to protons to impede the acceleration. In addition, according to Eq. (8), when $\boldsymbol{J} \neq 0$, the LG beam will generate a changing longitudinal electric field varying with $(l-\sigma)\varphi$, which may hinder the formation of the uniform electron layer during the "hole boring" stage when laser irradiating on the plasma.[31] Thus, an LG laser of $l = 1$, $p = 0$, $\sigma = 1$ is applied in our simulations.

3. Simulation results

To achieve efficient ion acceleration using an LG laser pulse with an NCD plasma, we have carried out a series of two-dimensional (2D) particle-in-cell (PIC) simulations using the code EPOCH.[38] The CP laser pulse has a wavelength of $\lambda = 1$ μm. The amplitude profiles of LG and Gaussian laser are determined by Eq. (4). The normalized amplitude of the CP laser pulse $a_0' \simeq (I_0\lambda^2/2.74\times10^{18})^{1/2}$. In typical simulations, a 30-fs laser pulse has the amplitude a_0' from 60 to 120 and the beam waist size $w_0 = 3\lambda$. The wavefront of the laser pulse arrives at the vacuum-foil interface $x = 10\lambda$ at $t = 0$. The semi-infinite NCD target is composed of protons H^+ and electrons e^- with a uniform density profile. The density $n_{\rm e}$ changes from $6n_{\rm c}$ to $10n_{\rm c}$ as the laser intensity increases. The critical density $n_{\rm c} = m_{\rm e}\omega^2/4\pi e^2$, ω is the angular frequency of the laser, $m_{\rm e}$ is the electron mass. In each simulation, a 45 μm×40 μm simulation box moves along the x axis at the speed of light and is divided into 3600×1600 cells. An NCD plasma is located at $x \geq 10\lambda$ and each cell has 50 macro-particles in the plasma region. Besides, the LG laser and Gaussian laser use the same laser amplitude a_0, which has the following conversion relationship with the input LG laser amplitude a_0': $a_0 \simeq 0.63a_0'$.

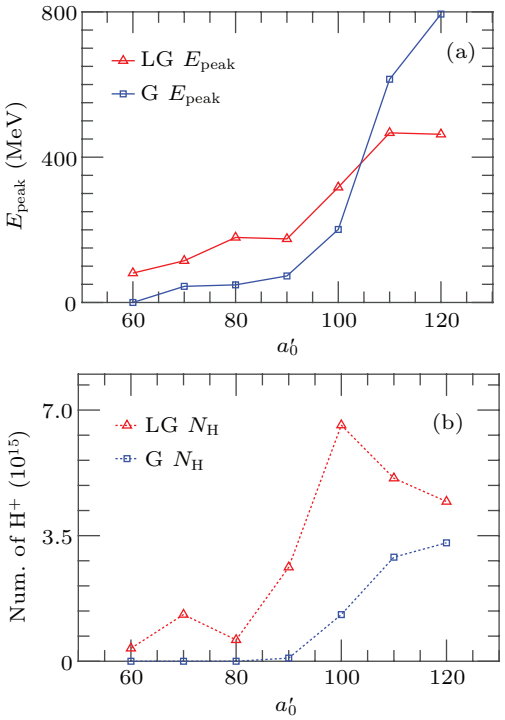


Fig. 1. The proton peak energy $E_{\rm peak}$ (a) and the corresponding proton yield $N_{\rm H}$ in energy peak (b). The red triangle lines are the interaction of LG with NCD plasma; the blue square lines are the cases for Gaussian beam. The laser beam waist $w_0 = 3\lambda$, and the input laser amplitude a_0 and the plasma density $n_{\rm e}$ are taken as (60, $6n_{\rm c}$), (70, $7n_{\rm c}$), (80, $7n_{\rm c}$), (90, $9n_{\rm c}$), (100, $10n_{\rm c}$), (110, $10n_{\rm c}$), and (120, $10n_{\rm c}$), respectively. We counted the protons at $|y| \leq 3\lambda$ in panel (b).

Simulation results show that quasi-monoenergetic proton beams are generated when LG lasers with intensities of 3.9×10^{21} W·cm^{-2}–1.6×10^{22} W·cm^{-2} interact with an NCD plasma, and the energy peak of the proton beam increases as the growth of laser amplitude a_0. Figure 1(a) indicates that the energy peak $E_{\rm pdak}$ increases from 81 MeV to 463 MeV when a_0' varies from 60 to 120 (correspondingly $a_0 = 40$–76 for LG laser pulse), and also the proton yield in the energy peak increases, as shown by Fig. 1(b). However, there is no quasi-monoenergetic peak generated or much lower peak energy for the Gaussian laser at $a_0' \leq 105$ interacting with an NCD plasma. And the proton numbers in energy peaks are obviously lower than those in the LG laser, e.g., the proton numbers in peak for Gaussian laser is one-fifth that of LG laser at $a_0' = 100$, as shown in Fig. 1(b). Besides, although the energy peak generated by a Gaussian laser can reach up to 803 MeV at $a_0' = 120$, which is higher than the one of LG laser, the protons yield in energy peak is always lower than that of LG laser.

To further analyze the proton acceleration driven by the LG laser in an NCD plasma, we display the distribution of the longitudinal electrostatic field E_x and the proton density.

At the beginning ($t = 10T_0$) of the LG laser interaction with NCD plasma, as shown in Figs. 2(a) and 2(c), E_x presents three peaks and the two sides are higher. This is because the hollow distribution of LG laser provides the ponderomotive force of $F_{y,\mathrm{LG}} \propto -\partial |E_\perp|^2 / \partial y = 2\partial |E_\perp|^2 (2y^2/w_0^2 - 1)/y$ according to Eqs. (6) and (7), which is inward when $|y| < w_0/\sqrt{2}$, while becoming outward when $|y| > w_0/\sqrt{2}$. Not only that, but the laser field is non-zero at the center due to the small focal spot ($w_0 = 3\lambda$) of LG laser. Thus, the electrons are pushed forward and meanwhile are compressed to the laser propagation axis by the ponderomotive force at the region of $|y| < w_0/\sqrt{2}$. Consequently, the inducing charge-separated field accelerates and accumulates amounts of protons in the region of $|y|\,1.5\lambda$. As the propagation of LG laser in an NCD plasma, the distribution of E_x characterized by an inward bowl-shape, as shown by Fig. 2(e), further accumulates the accelerated protons to the center. In contrast, Gaussian laser excites a laterally divergent E_x because the pondermotive force of Gaussian laser is $F_{y,\mathrm{G}} \propto -\partial |E_\perp|^2 / \partial y = 4|E_\perp|^2 y/\omega$, which is transverse gradient. Thus, both the electrons and protons are bend and defocus, and subsequently, only a few protons are efficiently accelerated around the wavefront, as shown in the following Figs. 2(f) and 2(h).

To characterize the accelerating field E_x excited by LG laser and Gaussian laser in an NCD plasma, we compare the spatialtemporal evolution of E_x and proton density n_H in Fig. 3. Figures 3(a) and 3(c) indicate that the longitudinal electric field E_x excited by LG laser has a greater intensity at $y = 3\lambda$ than that at the position of $y = 0$ due to the hollow distribution of laser field according to Eqs. (6) and (7). Furthermore, the propagating velocities of E_x at $y = 0$ and $y = 3\lambda$ both reach up to $0.6c$ (deriving from the slope of Figs. 3(a) and 3(c), and then decrease to about $0.2c$. These similar temporal evolutions of E_x maintain the inward bowl-shape distribution in Fig. 2(e), which efficiently prompt lots of accelerated protons to accumulate around the laser propagating axis ($y = 0$), as shown by Fig. 3(e). On the contrary, figures 3(b) and 3(d) show that E_x excited by Gaussian laser has the highest intensity at $y = 0$, while decreases quickly at $y = 3\lambda$. And also, the propagating velocity can reach up to $0.7c$ at $y = 0$, which is much higher than the one at $y = 3\lambda$. As a result, by combining Figs. 2(h), 3(f), and 3(h), the stable accelerating field cannot maintain for a long duration, and thus the protons are expelled transversely rather than efficiently accelerated around the wavefront of Gaussian laser.

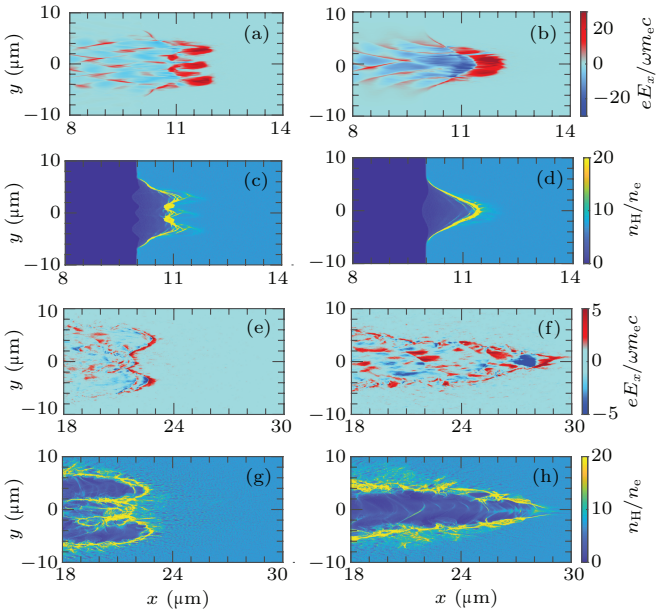


Fig. 2. Spatial distribution of the longitudinal electrostatic field E_x [(a), (b), (e), (f)] and proton density $n_\mathrm{H}/n_\mathrm{c}$ [(c), (d), (g), (h)]. The comparisons of LG laser and Gaussian laser at $t = 10T_0$ are taken as [(a), (c)] and [(b), (d)]; the comparisons of LG laser and Gaussian laser at $t = 45T_0$ are taken as [(e), (g)] and [(f), (h)]. The laser amplitude a_0' and target density n_e are taken as (70, $7n_\mathrm{c}$).

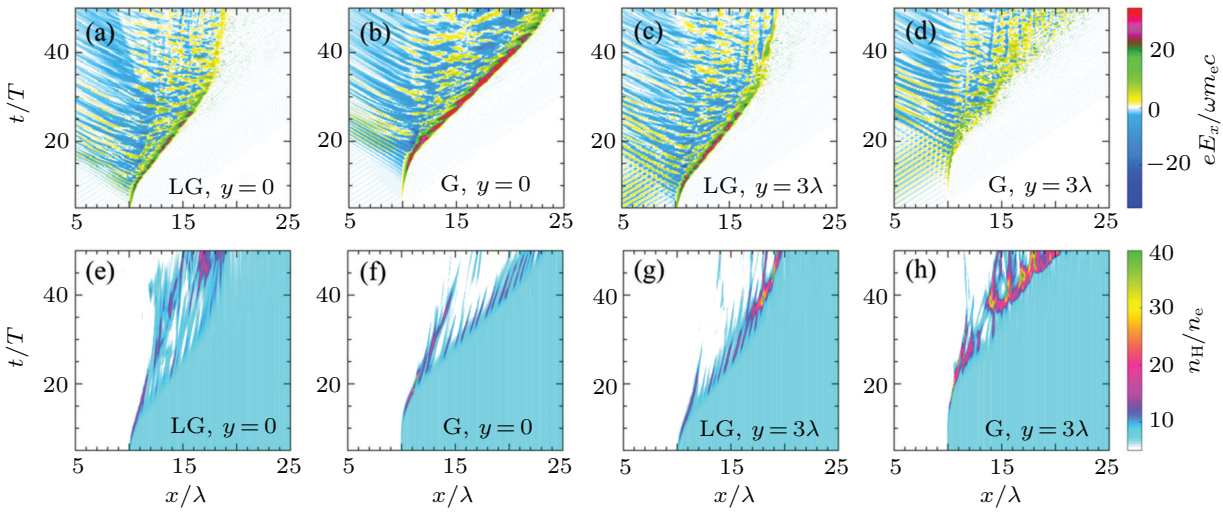


Fig. 3. The temporal evolution of longitudinal electrostatic field distribution E_x [(a)–(d)] and proton density distribution n_H [(e)–(h)]. Panels [(a), (e)] and [(b), (f)] present the spatialtemporal evolutions of field at $y = 0$ for LG laser and Gaussian laser, respectively. Panels [(c), (g)] and [(d), (h)] present the spatialtemporal evolutions of field at $y = 3\lambda$ for LG laser and Gaussian laser, respectively. The laser plasma parameters are the same as those in Fig. 2.

Since an inward bowl-shape longitudinal electrostatic field, excited by the hollow field of LG laser, can move forward and maintain its spatial distribution for dozens of laser duration, the protons can be efficiently accelerated and centered. A proton beam with an energy peak of $E_{\rm pdak} \simeq 115$ MeV is generated. The root-mean-square energy spread of this peak energy is about $\sigma \simeq 4.25$ due to the FWHM $= 2\sqrt{2\ln 2}\sigma$, and the corresponding divergence angle is $\theta < 5^\circ$, as shown in Fig. 4(a). In contrast, due to the repulsion to the protons by the outward pondermotive force of Gaussian laser, as shown in Fig. 4(b), no high-energy proton was observed and the protons are dramatically divergent. We also show the phase space p_x–x of protons for LG laser and Gaussian laser, as shown by Figs. 4(c) and 4(d), and the converged protons at $|y| \leq 3\lambda$ for LG laser is accelerated to $p_{\rm i} \geq 0.2 m_{\rm i} c$ based on hole-boring radiation pressure.[39,40]

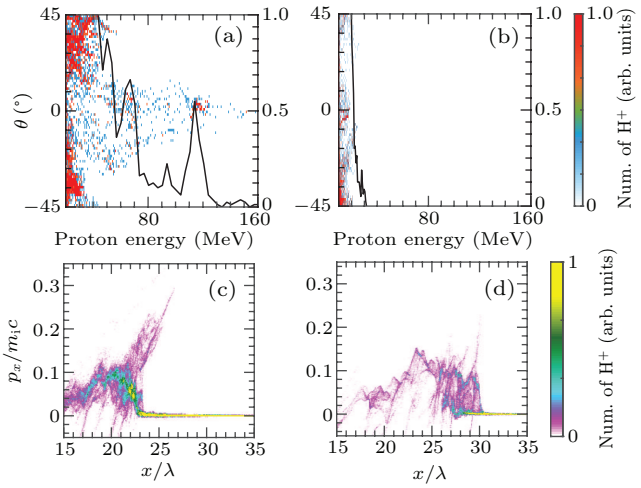


Fig. 4. The comparison of the proton energy–angle ($\theta = \arctan(v_y/v_x)$) between LG laser pulse (a) and Gaussian laser pulse (b) at $t = 55T_0$. Panels (c) and (d) are the corresponding phase space p_x–x of protons. We counted the protons at $|y| \leq 3\lambda$ and the laser plasma parameters are the same as those in Fig. 2.

Besides, only by increasing the laser intensity to above 10^{22} W·cm^{-2} and enlarging the laser focal spot to $\omega_0 = 7\lambda$ we can get a quasi-monoenergetic peak of $E_{\rm pdak} \simeq 550$ MeV for Gaussian laser, as shown in Fig. 5(b). However, with the laser intensity ranging from 10^{21} W·cm^{-2}–10^{22} W·cm^{-2} available in the near future,[41,42] the LG laser pulse with small focal spot can excite a moving longitudinal electrostatic field in the NCD plasma with a bowl-shape distribution, achieving better proton acceleration.

We also employ the three-dimensional (3D) simulations when an LG laser with normalized amplitude of $a_0 = 100$ interacts with an NCD plasma of $n_{\rm e} = 10n_{\rm c}$. Figure 6(a) shows that the protons converged to the peak density of $n_{\rm e} \simeq 32n_{\rm c}$ at the center is a little lower than the peak density of $n_{\rm e} \simeq 50n_{\rm c}$ for 2D simulations. The corresponding energy peak of $E_{\rm i} \simeq 580$ MeV, as shown by Fig. 6(b), is higher than the peak of $E_{\rm i} \simeq 480$ MeV in Fig. 5(a).

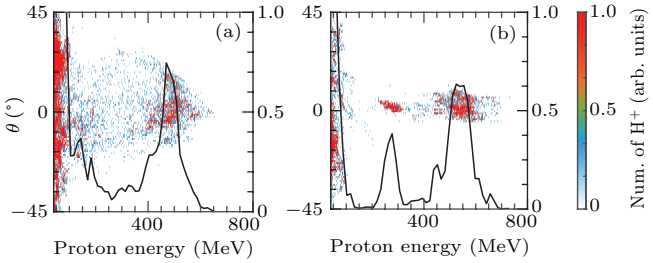


Fig. 5. The comparison of the proton energy–angle ($\theta = \arctan(v_y/v_x)$) between LG laser pulse (a) and Gaussian laser pulse (b) at $t = 55T_0$. We counted the protons at $|y| \leq 7\lambda$. The laser pulses have the focal spot size $w_0 = 7\lambda$, and the laser amplitude and target density are taken as (100, $10n_{\rm c}$).

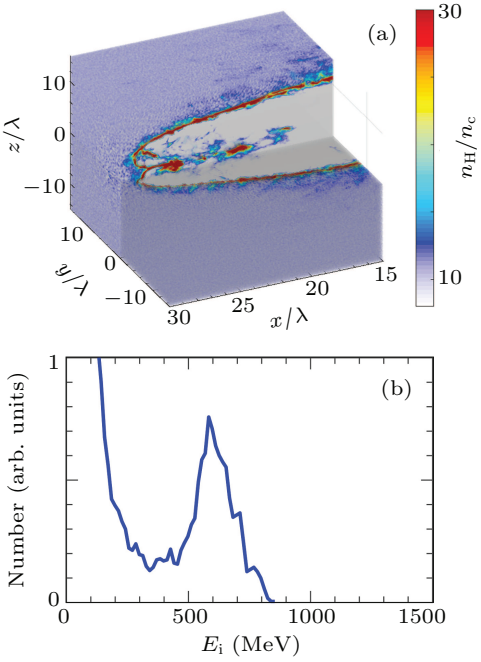


Fig. 6. The proton density distribution (a) and the corresponding energy spectra (b) at $t = 55T_0$ in 3D PIC simulations. The laser beam waist $w_0 = 5\lambda$, and the input laser amplitude a_0 and the plasma density $n_{\rm e}$ are taken as (100, $10n_{\rm c}$). We counted the protons at $|y| \leq 5\lambda$ in panel (b).

4. Conclusion

In summary, we have investigated by PIC simulation that a quasi-monoenergetic proton beam can be efficiently generated for an LG laser pulse with 10^{21} W·cm^{-2}–10^{22} W·m^{-2} in an NCD plasma. With a suitable density range of an NCD plasma, the longitudinal electrostatic field excited by LG laser can maintain the distribution characterized by the inward bowl-shape for dozens of laser durations. In this way, the protons can be accelerated and converged simultaneously by the electrostatic field, and therefore, a low-divergence proton beam with a peak energy of 115 MeV was obtained for LG laser with $I_0 \simeq 5.3 \times 10^{21}$ W·cm^{-2}. Our simulations have shown that the protons with no or much lower quasi-monoenergetic peak energy are generated by the Gaussian laser with the same intensity. It is worth pointing out that this work could provide a reference for the efficient ion acceleration experiments with PW-class laser systems recently available.[41,42]

Acknowledgements

Project supported by the Strategic Priority Research Program of the Chinese Academy of Sciences (Grant No. XDA25050300), the National Natural Science Foundation of China (Grant No. 12205366), the National Key Research and Development Program of China (Grant No. 2018YFA0404801), the Fundamental Research Funds for the Central Universities (Grant No. 2020MS138), and the Research Funds of Renmin University of China (Grant No. 20XNLG01).

References

[1] Wagner F, Deppert O, Brabetz C, Fiala P, Kleinschmidt A, Poth P, Schanz V A, Tebartz A, Zielbauern B, Roth M, Stöhlker T and Bagnoud V 2016 *Phys. Rev. Lett.* **116** 205002

[2] Li A X, Qin C Y, Zhang H, Li S, Fan L L, Wang Q S, Xu T J, Wang N W, Yu L H, Xu Y, Liu Y Q, Wang C, Wang X L, Zhang Z X, Liu X Y, Bai P L, Gan Z B, Zhang X B, Wang X B, Fan C, Sun Y J, Tang Y H, Yao B, Liang X Y, Leng Y X, Shen B F, Ji L L, Li R X and Xu Z Z 2022 *High Power Laser Sci. Eng.* **10** e26

[3] Kim I J, Pae K H, Choi II W, Lee C L, Kim H T, Singhal H, Sung J H, Lee S K, Lee H W, Nickles P V, Jeong T M, Kim C M and Nam C H 2016 *Phys. Plasmas* **23** 070701

[4] Higginson A, Gray R J, King M, Dance R J, Williamson S D R, Butler N M H, Wilson R, Capdessus R, Armstrong C, Green J S, Hawkes S J, Martin P, Wei W Q, Mirfayzi S R, Yuan X H, Kar S, Borghesi M, Clarke R J, Neely D and McKenna P 2018 *Nat. Commun.* **9** 724

[5] Macchi A, Borghesi M and Passoni M 2013 *Rev. Mod. Phys.* **85** 751

[6] Fuchs J, Antici P, D'Humières E, Lefebvre E, Borghesi M, Brambrink E, Cecchetti C A, Kaluza M, Malka V and Manclossi M 2005 *Nat. Phys.* **2** 48

[7] Bulanov S V, Esirkepov T Z, Khoroshkov V S, Kuznetsov A V and Pegoraro F 2002 *Phys. Lett. A* **299** 240

[8] Roth M, Cowan T E, Key M H, Hatchett S P, Brown C, Fountain W, Johnson J, Pennington D M, Snavely R A, Wilks S C, Yasuike K, Ruhl H, Pegoraro F, Bulanov S V, Campbell E M, Perry M D and Powell H 2001 *Phys. Rev. Lett.* **86** 436

[9] Kitagawa Y, Mori Y, Komeda O, *et al.* 2015 *Phys. Rev. Lett.* **114** 195002

[10] Beg F N, Krushelnick K, Gower C, Torn S and Dangor A E 2002 *Appl. Phys. Lett.* **80** 3009

[11] Wang W Q, Yin Y, Zou D B, Yu T P, Yang X H, Xu H, Yu M Y, Ma Y Y, Zhuo H B and Shao F Q 2014 *Chin. Phys. Lett.* **31** 115201

[12] Snavely R A, Key M H, Hatchett S P, Cowan T E, Roth M, Phillips T W, Stoyer M A, Henry E A, Sangster T C, Singh M S, Wilks S C, Mackinnon A, Offenberger A, Pennington D M, Yasuike K, Langdon A B, Lasinski B F, Johnson J, Perry M D and Campbell E M 2000 *Phys. Rev. Lett.* **85** 2945

[13] Borghesi M, Mackinnon A J, Campbell D H, Hicks D G, Kar S, Patel P K, Price D, Romagnani L, Schiavi A and Willi O 2004 *Phys. Rev. Lett.* **92** 055003

[14] Zepf M, El C, Fn B, Rj C, Ae D, Gopal A, Krushelnick K, Pa N, Tatarakis M and Wagner U 2003 *Phys. Rev. Lett.* **90** 064801

[15] Ban H Y, Gu Y J, Kon Q, L Y Y, Zhu Z and Kawata S 2012 *Chin. Phys. Lett.* **29** 035202

[16] Cowan T E, Fuchs J, Ruhl H, *et al.* 2004 *Phys. Rev. Lett.* **92** 204801

[17] Weng S M, Liu M, Sheng Z M, Murakami M, Chen M, Yu L L and Zhang J 2016 *Sci. Rep.* **6** 22150

[18] Dromey B, Kar S, Bellei C, Carroll D C, Clarke R J, Green J S, Kneip S, Markey K, Nagel S R, Simpson P T, Willingale L, McKenna P, Neely D, Najmudin Z, Krushelnick K, Norreys P A and Zepf M 2007 *Phys. Rev. Lett.* **99** 85001

[19] Kar S, Ahmed H, Prasad R, Cerchez M, Brauckmann S, Aurand B, Cantono G, Hadjisolomou P, Lewis C L S, Macchi A, Nersisyan G, Robinson A P L, Schroer A M, Swantusch M, Zepf M, Willi O and Borghesi M 2016 *Nat. Commun.* **7** 10792

[20] Dover N P, Cook N, Tresca O, Ettlinger O, Maharjan C, Polyanskiy M N, Shkolnikov P, Pogorelsky I and Najmudin Z 2016 *J. Plasma Phys.* **82** 415820101

[21] Marquè J R, Loiseau P, Bonvalet J, Tarisien M, d'Humières E, Domange J, Hannachi F, Lancia L, Larroche O, Nicolaï P, Puyuelo-Valdes P, Romagnani L, Santos J J and Tikhonchuk V 2021 *Phys. Plasmas* **28** 023103

[22] Puyuelo Valdes P, Henares J L, Hannachi F, Ceccotti T, D Domange J, Ehret M,d'Humieres E, Lancia L, Marquès J R, Ribeyre X, Santos J J, Tikhonchuk V and Tarisien M 2019 *Phys. Plasmas* **26** 123109

[23] Deng Y, Zhang Q, Yue D, Wei W, Feng L, Cui Y, Ma Y, Lu F, Yang Y, Huang Z, Wu Y, Zhou W, Weng S, Liu F, Chen M, Yuan X and Zhang J 2022 *Phys. Plasmas* **29** 123103

[24] Helle M H, Gordon D F, Kaganovich D, Chen Y, Palastro J P and Ting A 2016 *Phys. Rev. Lett.* **117** 165001

[25] Zhang H, Shen B F, Wang W P, Zhai S H, Li S S, Lu X M, Li J F, Xu R J, Wang X L, Liang X Y, Leng Y X, Li R X and Xu Z Z 2017 *Phys. Rev. Lett.* **119** 164801

[26] Longman A, Salgado C, Zeraouli G, Api naniz J I, Pérez-Hernández J A, Eltahlawy M K, Volpe L and Fedosejevs R 2020 *Opt. Lett* **45** 2187

[27] Wang W P, Dong H, Shi Z Y, Leng Y X, Li R X and Xu Z Z 2022 *Appl. Phys. Lett.* **121** 214102

[28] Wang W P, Shen B F, Zhang X M, Zhang L G, Shi Y and Xu Z Z 2015 *Sci. Rep.* **5** 8274

[29] Kogelnik H W and Li T 1966 *Appl. Opt.* **5** 1550

[30] Forbes A, Dudley A and Mclaren M 2016 *Adv. Opt. Photon.* **8** 200

[31] Pae K H, Song H, Ryu C M, Chang H N and Kim C 2020 *Plasma Phys. Control. Fusion* **62** 055009

[32] Torres J P and Torner L 2011 *Twisted Photons: Applications of Light with Orbital Angular Momentum* (Weinheim: WileyVCH), pp. 1–24

[33] Hu L X, Yu T P, Sheng Z M, Vieira J, Zou D B, Yin Y, McKenna P and Shao F Q 2018 *Sci. Rep.* **8** 7282

[34] Gbur G J 2011 *Mathematical Methods for Optical Physics and Engineering*

[35] Padgett M, Courtial J and Allen L 2004 *Phys. Today* **57** 35

[36] Allen L, Beijersbergen M W, Spreeuw R J C and Woerdman J P 1992 *Phys. Rev. A* **45** 8185

[37] He H, Friese M E J, Heckenberg N R and Rubinsztein-Dunlop H 1995 *Phys. Rev. Lett.* **75** 826

[38] Arber T D, Bennett K, Brady C S, Lawrence-Douglas A, Ramsay M G, Sircombe N J, Gillies P, Evans R G, Schmitz H, Bell A R and Ridgers C P 2015 *Plasma Phys. Control. Fusion* **57** 113001

[39] Robinson A P L, Kwon D H and Lancaster K 2009 *Plasma Phys. Control. Fusion* **51** 095006

[40] Weng S M, Murakami M, Mulser P and Sheng Z M 2012 *New J. Phys.* **14** 063026

[41] Yoon J W, Jeon C, Shin J, Lee S K, Lee H W, Choi I W, Kim H T, Sung J H and Nam C H 2019 *Opt. Express* **27** 20412

[42] Danson C N, Haefner C, Bromage J, *et al.* 2019 *High Power Laser Sci. Eng.* **7** e54